Supplementary Information

Triplet Excitation Dynamics of Photosynthetic Light-Harvesting Antennae: Mechanistic Insights into the Conjugation Regulated Carotenoid Functionality

Yu-Qian Li,[a] Yi-Hao Yan,[bc] Rong-Yao Gao,[a] Jian-Wei Zou,[d] Yu-Lu Wu,[bc] Xing-Yu Yue,[bc] Yao Lu,[a] Xiang-Ping Wang,[bc] Ming-Qing Chen,[a] Qi-Wei Li,[a] Hao-Yi Wang,[a] Peng Wang,[a] Long-Jiang Yu,*[bc] Junrong Zheng,[d] Jian-Ping Zhang*[a]

[a]Key Laboratory of Advanced Light Conversion Materials and Biophotonics, School of Chemistry and Life Resources, Renmin University of China, Beijing 100872, P. R. China
[b]Photosynthesis Research Center, Key Laboratory of Photobiology, Institute of Botany, Chinese Academy of Sciences, Beijing 100093, P. R. China
[c]University of Chinese Academy of Sciences, Beijing 100049, P. R. China
[d]College of Chemistry and Molecular Engineering, Beijing National Laboratory for Molecular Sciences, Peking University, Beijing 100871, China

Email: longer@ibcas.ac.cn (L.-J. Yu); jpzhang@ruc.edu.cn (J.-P. Zhang)

S1.MATERIALS AND METHODS

Sample Preparation. The LH2 complexes from *Rba. sphaeroides* G1C, *Rba. sphaeroides* 2.4.1, *Thermochromatium* (*Tch.*) *tepidum* and *Rhodopseudomonas* (*Rps.*) *palustris* were prepared following previously reported protocols.[S1–S4] The LH1-RC complexes from *Tch. tepidum* and *Rsp. rubrum* were prepared as described in Refs S5 and S6. The LH1-only complex from *Tch. tepidum* and the LH1-RC complex from *Rfl. castenholzii* were prepared according to Refs S7 and S8, respectively. The LH1′ and LH1-RC complexes from *Rss. parvum* 930I were prepared following the procedures described in Ref S9. The anaerobic condition of the LH samples for time-resolved spectroscopic measurement was achieved by adding 20 mM β-D-glucose, 5 U/mL glucose oxide and 5 U/mL catalase into the sample solutions, and the adaption time was 15 min.

Steady-State and Time-Resolved Spectroscopies. Optical absorption spectra were measured with a Cary 60 spectrophotometer (Agilent Technologies, Santa Clara, CA). Resonance Raman spectra were measured under laser excitation at 532 nm with a XploRA PLUS spectrometer (Horiba, Japan).

The apparatus for measuring the *ns*-TA spectra up to a delay time of ~150 ns is described below. The pump pulses were provided by a Q-Switched Nd:YVO_4 laser (532 nm, 800 ps; Picolo AOT MOPA, InnoLas Laser), and the white-light supercontinuum probe was obtained by focusing the femtosecond pulses from a regenerative amplifier (800 nm, 120 fs; SPTF-100F-KHPR, Spectra-Physics) into water. A digital delay generator (SRS DG535, Stanford Research System) was used to regulate the delay time between pump and probe pulses. The pump was chopped to a half repetition rate of the probe. The difference absorption (ΔOD) signal was detected by a spectrometer (AvaSpec-UL2048×64-EVO, Avantes), and the ΔOD spectra were calculated from a pair of consecutive probe pulses with pump ON and OFF, respectively. The ΔOD detection sensitivity was better than 10^{-4} after averaging 1,000 ON-OFF cycles. The kinetics of the $S_n \leftarrow S_1$ excited state absorption (ESA) of all-*trans* Lyc diluted in toluene was taken as the instrumental response function (IRF), which is reasonable in view of the ultrashort S_1-state lifetime (~5 ps). The time resolution was about 1.43 ns as determined from the full width at half maximum (FWHM) of the IRF.

The time-resolved ΔOD spectra in the temporal regime of 0~100 μs were measured with a time resolution of 50 ns by using an independent setup, and the protocol for constructing a triplet excitation profile (TEP) was described elsewhere.[S10,S11] Briefly, the excitation wavelength (λ_{ex}) was tuned systematically to cover the interested spectral region of sample absorption, and the ^{3}Car* kinetics were probed at the maximal ESA wavelength of ^{3}Car*. The TEP spectra of the LHs were constructed by plotting the maximal ESA amplitudes in the kinetic traces (typically at ~100 ns) as a function of λ_{ex}. Since the excitation pulse energy was kept constant upon varying λ_{ex}, a TEP can be regarded as an actinic spectrum of ^{3}Car*, reflecting the overall relative yields of ^{3}Car* at different λ_{ex}.

The *fs*-TA spectrometer is described briefly below.[S12] An optical parametric amplifier (TOPAS-Prime, Light Conversion Ltd., Vilnius, Lithuania) driven by the output from a regenerative amplifier (120 fs, 792 nm, 1 kHz; Uptek Solutions Inc., NY) provided the pump light at a desired λ_{ex} with a pulse duration of 60 fs (FWHM). The supercontinuum white-light probe was generated by focusing a small portion of the regenerative amplifier output into with a sapphire plate (5 mm thickness). A magic angle (54.7°) was set between the polarization of the pump and probe light. The ΔOD signal was collected in a shot-to-shot manner by using a fast spectrometer equipped with a CMOS detector (Tiger-Vis-4K, Tiger Instruments), and the *fs*-TA spectra were corrected against group velocity dispersion.

In the TA measurements, the sample OD was adjusted to 0.3~0.5 at λ_{ex} in terms of an optical pathlength of 1 mm. The excitation photon fluence was kept below 1×10^{14} photons·cm^{-2}·pulse^{-1}, so as to minimize the unwanted nonlinear response. The steady-state absorption spectra of the LH samples before and after measurement were compared, and no significant sample degradation was recognized. All of the spectroscopic measurements were carried out at room temperature (295 K). Curve fitting programs were coded on the basis of Matlab2020a (MathWorks, Natick, MA), and the freeware Glotaran[S13] was used for the global analysis of the TA spectra

S2. Structures of Bacterial Light-Harvesting Complexes (LHs)

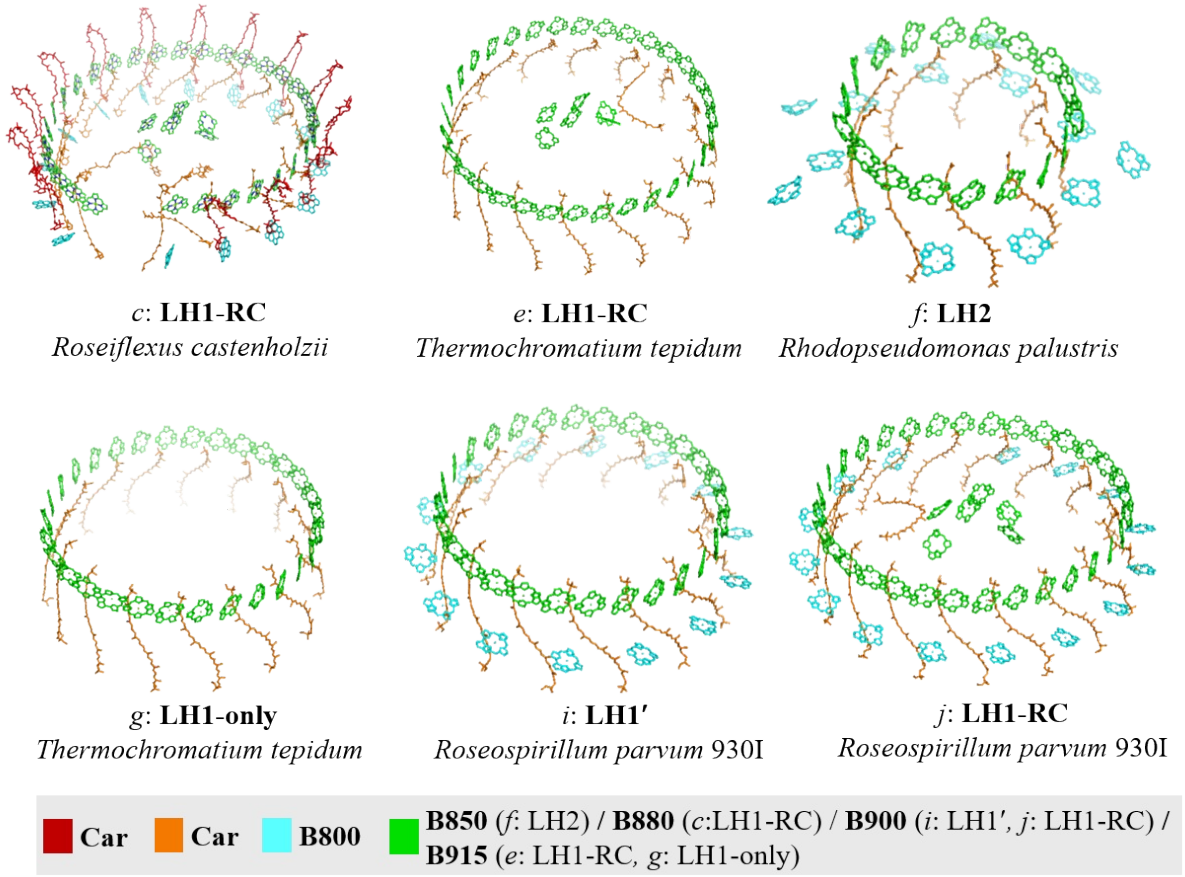

Figure S1. Schematic illustration of the LH structures. *c*: *Rfl. castenholzii* LH1-RC (2.86 Å/3.1 Å; PDB codes 8IUG/8J5P),[S14,S15] *e*: *Tch. tepidum* LH1-RC (1.9 Å; PDB code 5Y5S),[S5] *f*: *Rps. palustris* LH2 (2.7 Å; PDB code 7ZCU),[S4] *g*: *Tch. tepidum* LH1-only (3.11 Å; PDB code 8JC8),[S7] *i*: *Rss. parvum* 930I LH1′ (2.35 Å; PDB code 8ZJW),[S9] *j*: *Rss. parvum* 930I LH1-RC (2.65 Å; PDB code 8ZK2),[S9] For clarity, α,β-polypeptides of LH and RC were omitted, and the phytol chain of BChl *a* was truncated. Indexes for bacterial LHs (*c*, *e*, *f*, *g*, *i*, *j*) are used throughout the paper.

S3. Carotenoid Composition Analysis for LHs

Pigments were extracted from whole cells with 200 µL of acetone/methanol (7:2, v/v), and then dried in vacuo. The extract was dissolved in 100 µL of acetone/ methanol (7:2, v/v) at room temperature, and a 2 µL aliquot of this solution was subjected to ultrahigh performance combined phase chromatography-mass spectrometry (UPCC-MS) analysis. All manipulations were performed in the dark. For quantitative analysis, the molar extinction coefficient at the maximal wavelength of each Car in the UPCC eluent of methanol was assumed to be the same. UPC2-MS/MS analysis for anthocyanins was performed using an ACQUITY Ultra Performance Supercritical Liquid Chromatograph (UPC2 I-CLASS, Waters) coupled with a Xevo™ TQ-MS triple quadrupole mass spectrometer (Waters, Milford, USA). Chromatographic separation was performed on an ACQUITY UPLC® HSS C18 SB column (3×100 mm, 1.8 µm internal diameter) at a flow rate of 1.5 mL min^{-1} at 40 °C. The elution solvent comprised A (CO_2) and B (ethanol). A gradient elution protocol was performed as follows: 5% B at 0 min, 10% B at 9 min, 20% B at 12 min, 5% B at 13 min, and 5% B at 15 min. MS detection conditions were as follows: positive ion model; capillary voltage, 3 kV; cone voltage, 20 V; desolvation temperature, 400 °C; source temperature, 150 °C; desolation gas flow, 800 L/h; collision gas flow, 0.14 mL/min; collision energy, 2 eV; scan range 380–1000 (m/z).

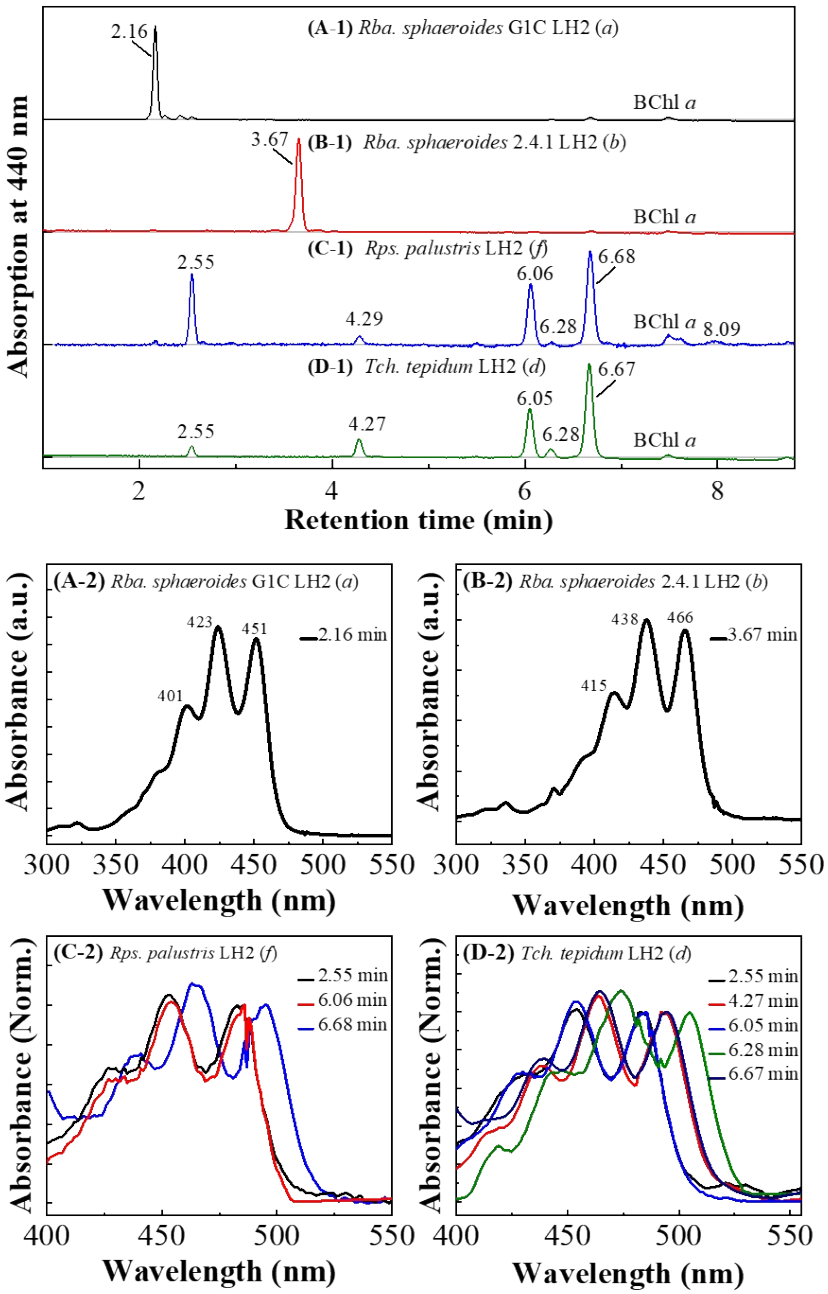

Figure S2. HPLC chromatograms and corresponding UV-visible absorption spectra of the pigment extracts of the LH2 complexes from different bacterial species. (**A-1,2**) *a*: *Rbs. Spaeroides* G1C, (**B-1,2**) *b*: *Rbs. Spaeroides* 2.4.1, (**C-1,2**) *f*: *Rps. palustris*, (**D-1, 2**) *d*: *Tch. tepidum*. The detection wavelength was 440 nm. The Car compositions are listed in Table S1.

Table S1. Car compositions (in %) of LH2, LH1-only and LH1-RC complexes from various bacterial species.

Index	LH complex (bacterium)	Car ($n_{c=c}$) (*)									References
		Neu (9)	Sph (10)	Lyc (11)	Rhp (11)	γ-Car (11)	Did (12)	Anh (12)	Rhv (12)	Spi (13)	
a	LH2 (*Rba. sphaeroides* G1C)	>90.0									This work
b	LH2 (*Rba. sphaeroides* 2.4.1)		>90.0								This work
c	LH1-RC (*Rfl. castenholzii*)					>88.0					S16
d	LH2 (*Tch. tepidum*)			3.4	26.1		52.2	12.6		5.8	This work
e	LH1-RC (*Tch. tepidum*)									>90.0	S17
f	LH2 (*Rps. palustris*)			21.4	30.4		42.9	4.5	0.9	0.01	This work
g	LH1-only (*Tch. tepidum*)			1.4	4.4		0.7	37.7	6.4	49.4	S7
h	LH1-RC (*Rsp. rubrum*)									>90.0	S18
i	LH1′ (*Rss. parvum* 930I)									>90.0 (**)	S19
j	LH1-RC (*Rss. parvum* 930I)									>90.0 (**)	S19

(*)Abbreviation: Neu, neurosporene; Sph, spheroidene; Lyc, lycopene; Rhp, rhodopin; γ-Car, γ-carotene; Did, 3,4-didehydrorhodopin; Anh, anhydrorhodovibrin; Rhv, rhodovibrin; Spi, spirilloxanthin.
(**)Determined from intraplasmic membrane (ICM) fragments.

S4. Additional Steady-State Spectra of LHs

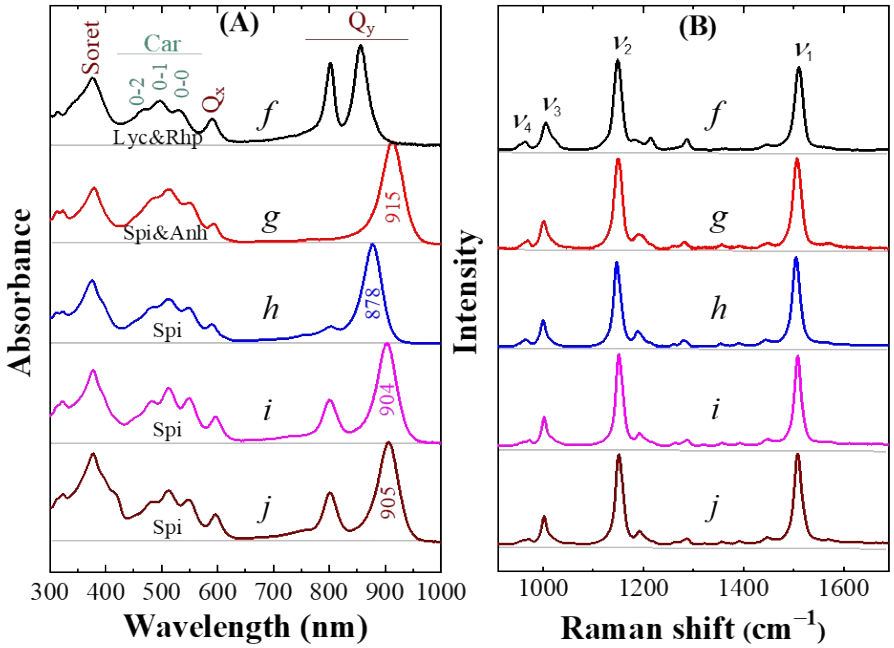

Figure S3. Steady-state optical spectra of LH2 and LH1-RC complexes at room temperature. (**A**) Ground-state absorption spectra normalized at Q_y maxima. (**B**) Raman spectra normalized at ν_1 maxima. The following indexes for bacterial LHs are used throughout the paper. *f*: *Rps. palustris* LH2; *g*: *Tch. tepidum* LH1-only; *h*: *Rsp. rubrum* LH1-RC; *i*: *Rss. parvum* 930I LH1′; *j*: *Rss. parvum* 930I LH1-RC. See Figure 2 of the main text for the steady-state spectra of the other LH2 and LH1-RC complexes (*a*–*e*).

S5. Additional *ns*-TA Spectra of LHs within 150 ns

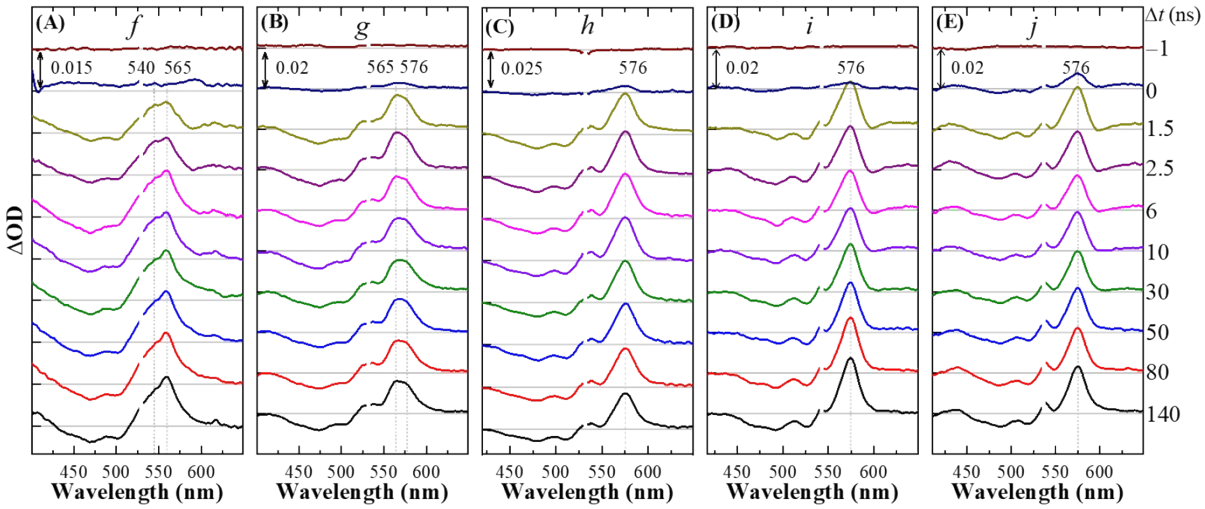

Figure S4. *ns*-TA spectra of LHs at selected delay times (Δ*t*). (**A**) *f*: *Rps. palustris* LH2, (**B**) *g*: *Tch. tepidum* LH1-only, (**C**) *h*: *Rsp. rubrum* LH1-RC, (**D**) *i*: *Rss. parvum* 930I LH1′, (**E**) *j*: *Rss. parvum* 930I LH1-RC. Indexes (*f*–*j*) are used though out the paper. See Figure 3 for the *ns*-TA spectra for the other bacterial LHs (*a*–*e*).

S6. Near-Infrared Fluorescence Kinetics of LHs.

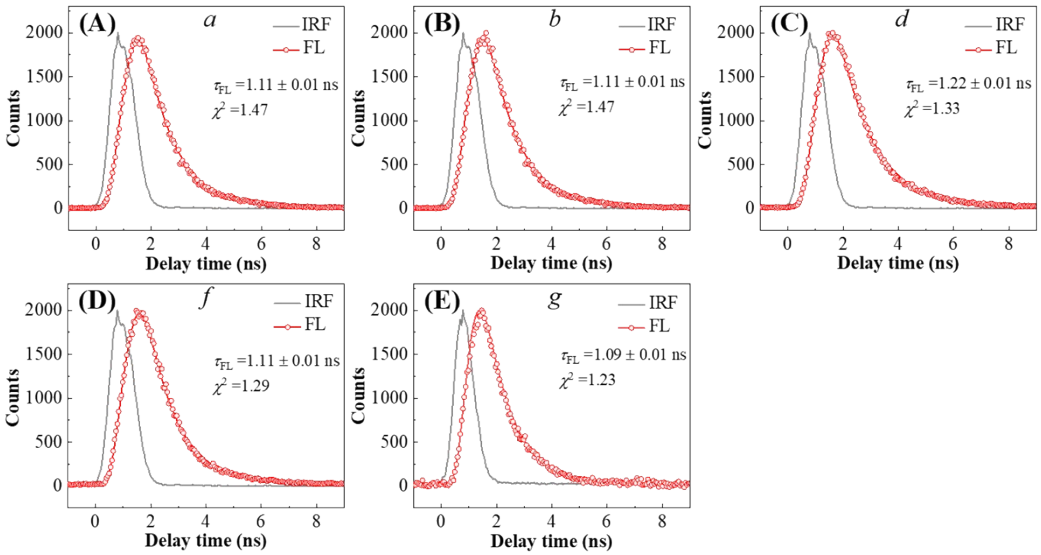

Figure S5. Fluorescence decay kinetics of the bacterial LHs at room temperature. The kinetics were probed at (**A**, **B**) 860 nm for *Rba. sphaeroides* G1C LH2 (*a*) and *Rba. sphaeroides* 2.4.1 LH2 (*b*), (**C**) 875 nm for *Tch. tepidum* LH2 (*d*), (**D**) 870 nm for *Rps. palustris* LH2 (*f*), and (**E**) 930 nm for *Tch. tepidum* LH1-only (*g*). Instrumental response functions (IRFs) are shown for reference. Solid lines in red are fitting curves derived on the basis of a mono-exponential model function, and the fitting goodness (χ^2) and fluorescence lifetime (τ_{FL}) are indicated in each panel. The kinetic traces were recorded on an FLS 980 spectrometer (Edinburgh Instruments, UK) equipped with a time-correlated single-photon counting (TCSPC) module. The photomultiplier tube (PMT) detector was R5509-73 (Hamamatsu Photonics, K. K., Japan). The maximal OD_{Qy} of a sample was ~0.04. The excitation wavelength was 475 nm (60 ps, 20 MHz). LH indexes (*a*, *b*, *d*, *f*, *g*) are used throughout the paper.

S7. Time-Resolved Car($T_n \leftarrow T_1$) Absorption Spectra in 0–100 μs

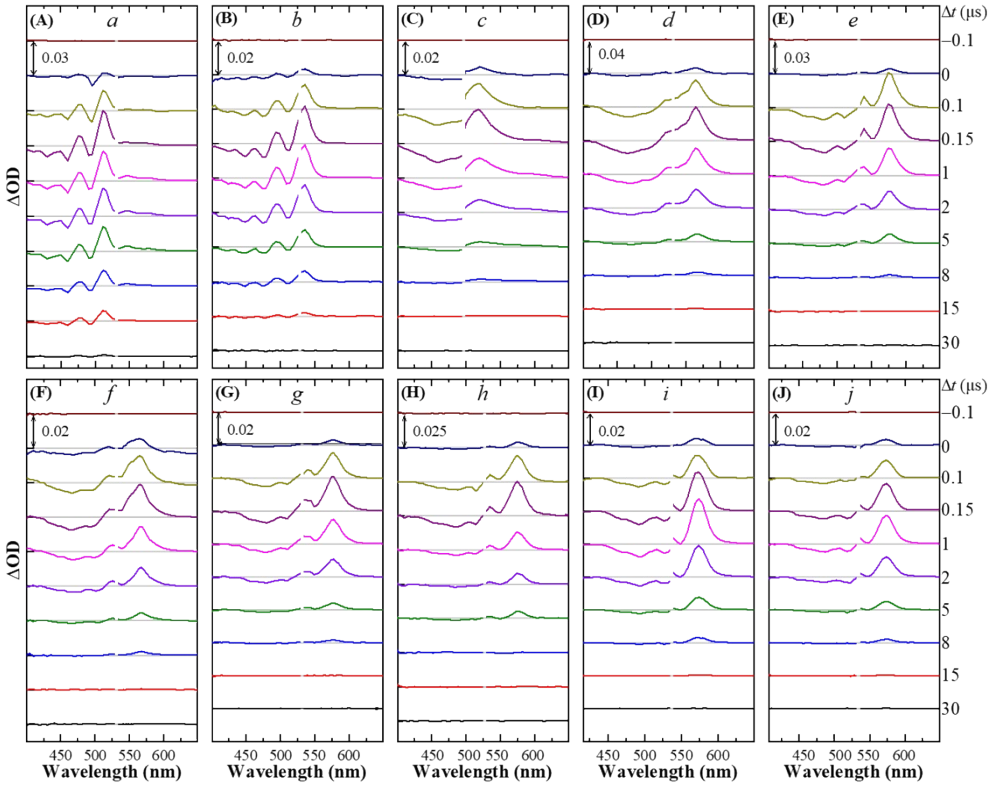

Figure S6. Time-resolved absorption spectra at representative delay time (Δ*t*) for the LHs under anaerobic condition. (**A**) *a*: *Rba. sphaeroides* G1C LH2, (**B**) *b*: *Rba. sphaeroides* 2.4.1 LH2, (**C**) *c*: *Rfl. castenholzii* LH1-RC, (**D**) *d*: *Tch. tepidum* LH2, (**E**) *e*: *Tch. tepidum* LH1-RC, (**F**) *f*: *Rps. palustris* LH2, (**G**) *g*: *Tch. tepidum* LH1-only, (**H**) *h*: *Rsp. rubrum* LH1-RC, (**I**) *i*: *Rss. parvum* 930I LH1′, (**J**) *j*: *Rss. parvum* 930I LH1-RC. The excitation wavelength was 532 nm except in the case of *Rfl. castenholzii* LH1-RC where it was 500 nm. The indexes (*a*–*j*) are used throughout the paper.

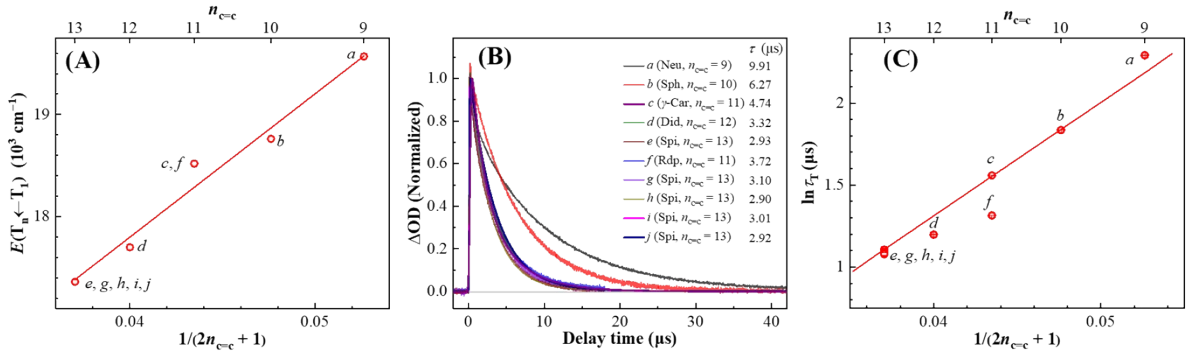

Figure S7. Car triplet excited state properties. (**A**) Plot of the Car(T_n←T_1) transition energy of the LHs against $1/(2n_{c=c}+1)$. The transition energy were converted from the Car(T_n←T_1) absorption maximal wavelengths as determined from the corresponding datasets in Figure S6. The solid line represents the fitting curve as described by the relation, $E_T(T_n←T_1) = 12.18 + 140.51×(1/(2n_{c=c}+1)$. (**B**) ^{3}Car* decay kinetics plotted at the Car(T_n←T_1) absorption maxima from the corresponding datasets of Figure S6. The lifetimes (τ_T) of ^{3}Car* were derived from the kinetic traces via exponential curve fitting. (**C**) Semilogarithmic plot of τ_T against $1/(2n_{c=c}+1)$. The solid line represents the fitting curve, $\ln \tau_T = -1.45 + 69.15×(1/(2n_{c=c} + 1)$. Indexes (*a*–*j*) are used throughout the paper. *a*: *Rba. sphaeroides* G1C LH2; *b*: *Rba. sphaeroides* 2.4.1 LH2; *c*: *Rfl. castenholzii* LH1-RC; *d*: *Tch. tepidum* LH2; *e*: *Tch. tepidum* LH1-RC; *f*: *Rps. palustris* LH2; *g*: *Tch. tepidum* LH1-only; *h*: *Rsp. rubrum* LH1-RC; *i*: *Rss. parvum* 930I LH1′; *j*: *Rss. parvum* 930I LH1-RC.

S8. *ns*-TA Kinetics Traces of LHs within 150 ns

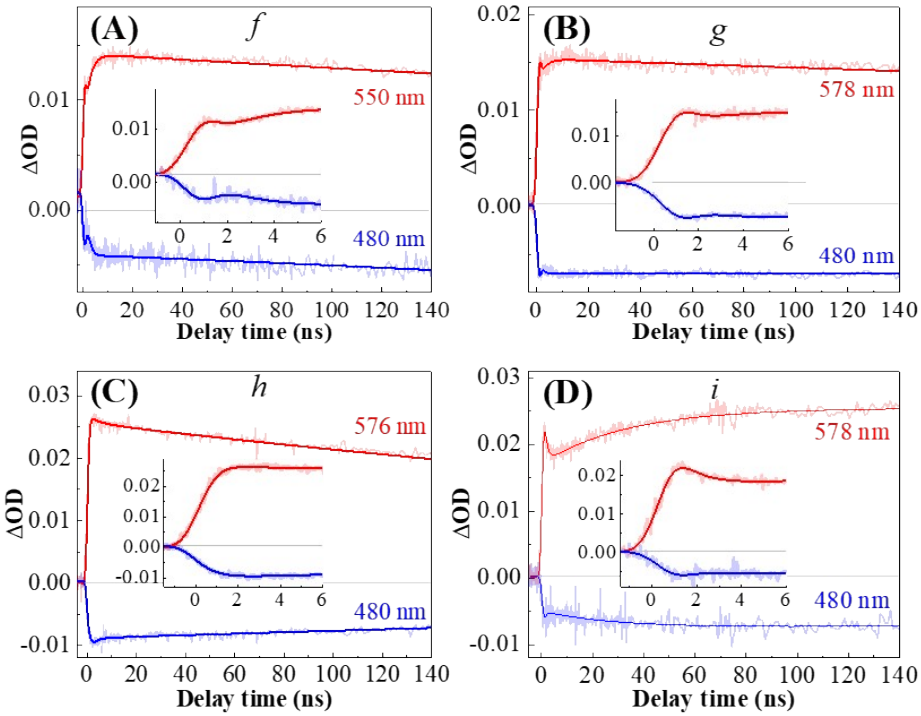

Figure S8. *ns*-TA kinetic traces for the LHs at the indicated probe wavelengths as plotted from the corresponding datasets of Figure S4. (**A**) *f*: *Rps. palustris* LH2, (**B**) *g*: *Tch. tepidum* LH1-only, (**C**) *h*: *Rsp. rubrum* LH1-RC, (**D**) *i*: *Rss. parvum* 930I LH1′. Insets show the details in the initial 6 ns. See Figure 4 for the kinetic traces of the other bacterial LHs (*a*–*e*, *j*). Indexes for the bacterial LHs (*f*–*i*) are used throughout the paper.

S9. Kinetics Parameters Derived from Curve Fitting of the *ns*-TA Kinetics within 150 ns

Table S2. Kinetics parameters derived by simultaneously fitting the kinetic traces at the indicated probing wavelengths λ_{pr} (cf. Figure 4 (*a*–*e*, *j*) of the main text and Figure S8 (*f*–*i*)) to a multiexponential model function.(*) The rise components in form of 1–exp(−*t*/τ) are indicated with '*r*' in parentheses, the decay components are in form of exp(−*t*/τ), A_i presents the preexponential factors, and τ_i associated with the 1–exp(−*t*/τ) components are regarded with the TET time constant (with Car as an energy acceptor).

Sample	λ_{pr} (nm)	A_1 (%)	τ_1 (ns)	A_2 (%)	τ_2 (ns)	A_3 (%)	τ_3 (ns)	A_4 (%)	τ_4
a	511 458	100 −100	1.82 ± 0.07	100 (*r*) −100 (*r*)	19.45 ± 0.16				
b	540 480	100 −100	1.85 ± 0.09	100 (*r*) −100 (*r*)	16.52 ± 0.15				
c	540 480	77.6(*r*) −71.4(*r*)	0.27 ± 0.04	6.5 −10.8	0.04 ± 0.00	23.4(*r*) −28.6(*r*)	13.69 ± 3.44	93.5 −89.2	4.74 (µs)
d	565 480	57.6 (*r*) −41.6(*r*)	0.17 ± 0.00	54.1 −44.4	0.33 ± 0.03	42.4 (*r*) −58.4(*r*)	3.34 ± 0.34	45.9 −55.6	3.32 (µs)
e	578 480	88.1 (*r*) −94.9(*r*)	0.11 ± 0.00	42.3 −42.9	0.16 ± 0.01	11.9 (*r*) −5.1 (*r*)	2.85 ± 0.02	57.7 −57.1	2.93 (µs)
f	550 480	75.9(*r*) −74.7(*r*)	0.02 ± 0.00	17.5 −16.7	0.27 ± 0.03	24.1 (*r*) −25.3(*r*)	3.85 ± 0.23	82.5 −83.3	3.72 (µs)
g	578 480	59.5 (*r*) −58.5(*r*)	0.09 ± 0.00	13.5 −11.8	0.15 ± 0.07	40.5 (*r*) −41.5(*r*)	2.42 ± 0.21	86.5 −88.2	3.10 (µs)
h	576 480	86.6 (*r*) −83.3(*r*)	0.07 ± 0.00	19.1 −17.9	0.20 ± 0.01	13.4 (*r*) −16.7(*r*)	2.02 ± 0.32	80.9 −82.1	2.90 (µs)
i	575 480	61.5 (*r*) −50.0(*r*)	0.22 ± 0.09	100 −100	0.48 ± 0.02	18.0 (*r*) −28.4(*r*)	1.59 ± 0.05	20.5 (*r*) −21.6(*r*)	31.2 ± 1.05 (ns)
j	575 480	46.7 (*r*) −48.8(*r*)	0.29 ± 0.07	100 −100	0.48 ± 0.10	14.2 (*r*) −22.5(*r*)	1.80 ± 0.09	39.2(*r*) −28.7(*r*)	51.8 ± 2.53 (ns)

*Model functions:
For *a*, *b*: $\Delta OD(t) = A_1 \cdot \exp(-t/\tau_1) + A_2 \cdot (1-\exp(-t/\tau_2))$;
For *c*–*h*: $\Delta OD(t) = A_1 \cdot (1-\exp(-t/\tau_1) + A_2 \cdot \exp(-t/\tau_2) + A_3 \cdot (1-\exp(-t/\tau_3) + A_4 \cdot \exp(-t/\tau_4)$;
For *i*, *j*: $\Delta OD(t) = A_1 \cdot (1-\exp(-t/\tau_1) + A_2 \cdot \exp(-t/\tau_2) + A_3 \cdot (1-\exp(-t/\tau_3) + A_4 \cdot (1-\exp(-t/\tau_4)$.

S10. BChl-Car Distances in LHs

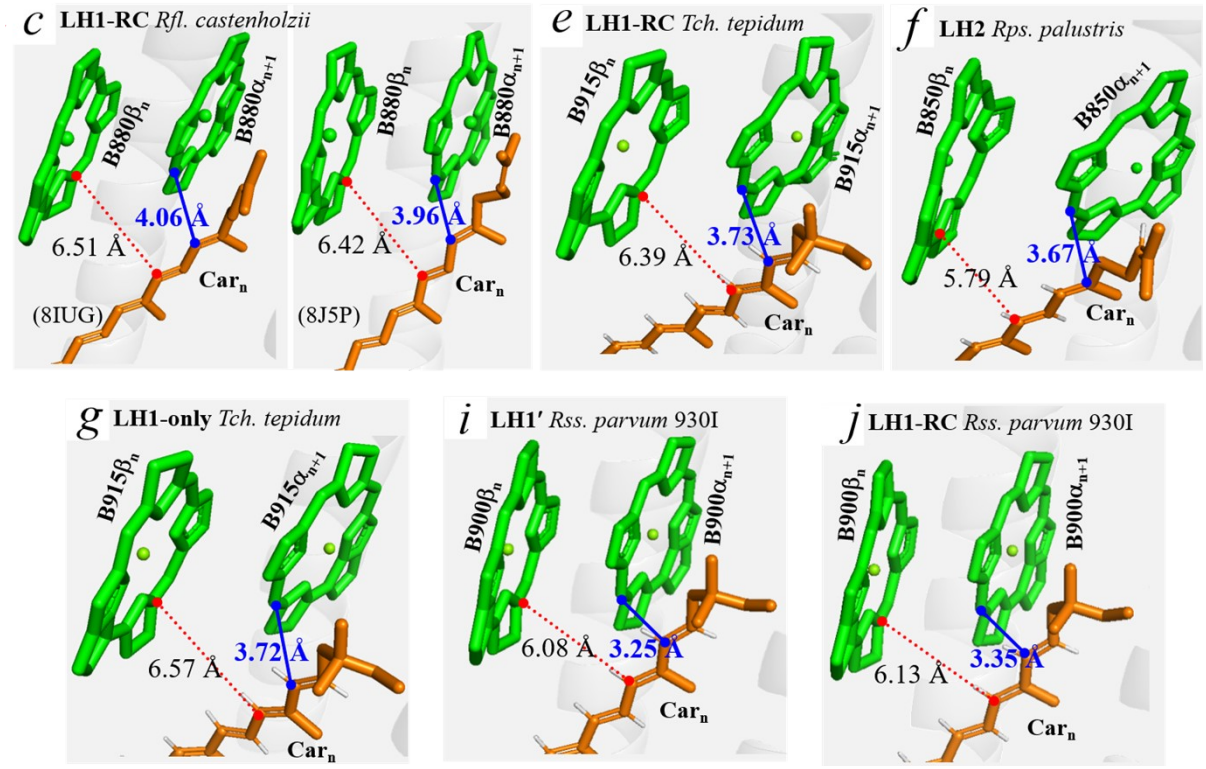

Figure S9. Comparison of the closest edge-to-edge distances between the conjugated backbones of Car and BChl. *c*: *Rfl. castenholzii* LH1-RC (PDB code, 8IUG/8J5P, 2.86 Å/3.1 Å),[S14, S15] *e*: *Tch. tepidum* LH1-RC (PDB code, 5Y5S, 1.9 Å),[S5] *f*: *Rps. palustris* LH2 (PDB code, 7ZCU, 2.7 Å),[S4] *g*: *Tch. tepidum* LH1-only (PDB code, 8JC8, 3.11 Å),[S7] *i*: *Rss. parvum* 930I LH1′ (2.35 Å; PDB code 8ZJW),[S9] *j*: *Rss. parvum* 930I LH1-RC (2.65 Å; PDB code 8ZK2).[S9]

S11. Time-Evolution Profiles Derived from Global Analysis

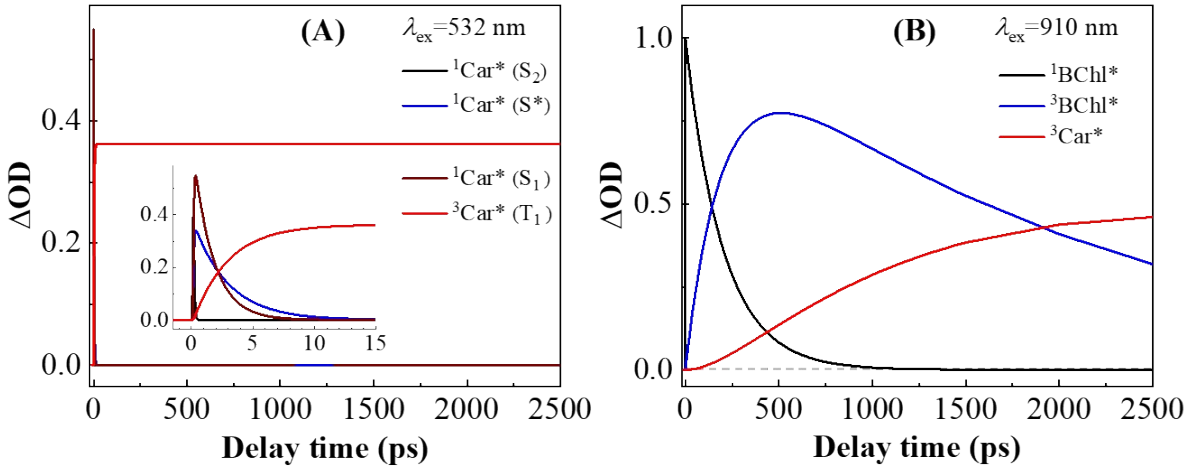

Figure S10. Temporal evolution profiles of *Tch. tepidum* LH1-RC (*e*). These kinetic results, under excitation wavelengths (λ_{ex}) of (**A**) 532 nm and (**B**) 910 nm, were derived by global fitting the *fs*-TA spectral datasets as shown in Figure 6A,B in the main text. See Figure 6C,D in the main text for the respective kinetics models used in target analysis, and for the species associated spectra (SASs).

S12. Conjugation-Length Dependent Car-to-BChl SET Efficiency

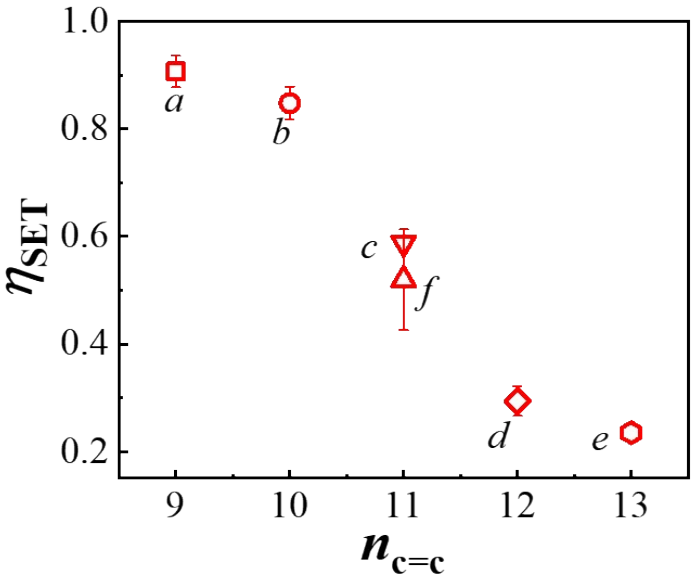

Figure S11. Plot of the overall efficiency of Car-to-BChl SET (η_{SET}) against Car conjugation length ($n_{c=c}$). The statistics of η_{SET} was based on the reported values (Table S3).

Table S3. List of literature-reported overall Car-to-BChl SET efficiency (η_{SET}) for the LHs from various bacterial species binding Cars with conjugation length ($n_{c=c}$) varying from 9 to 13.

Carotenoid ($n_{c=c}$)	LHs of Bacterial Species (index)	η_{SET} (%)[Ref]
Neurosporene (9)	LH2 of *Rhodobacter sphaeroides* G1C (*a*)	88[S20], 92[S21], 88[S22], 91[S23], 94[S24], 87[S25]
Spheroidene (10)	LH2 of *Rhodobacter sphaeroides* 2.4.1 (*b*)	84[S20], 89[S21], 83[S22], 93[S23], 82[S24]
γ-Car (11)	LH1-RC of *Roseiflexus castenholzii* (*c*)	58[S16]
Lycopene (11)	LH2 of *Rhodobacter sphaeroides* G1C	64[S26]
Rhodopin (11)		62[S26]
multi-compositional Cars (11-13)	LH2 of *Rhodopseudomonas palustris* (*f*)	23-26[S22],
multi-compositional Cars (11-13)	LH2 of *Thermochromatium tepidum* (*d*)	30[S27], 26[S28],
Spirilloxanthin (13)	LH1-RC of *Thermochromatium tepidum* (*e*)	23[S29], 20[S30]

References

(S1) Qian, P.; Swainsbury, D. J. K.; Croll, T. I.; Castro-Hartmann, P.; Divitini, G.; Sader, K.; Hunter, C. N. Cryo-EM Structure of the *Rhodobacter sphaeroides* Light-Harvesting 2 Complex at 2.1 Å. *Biochem*. **2021**, *60*, 3302−3314.

(S2) Qian, P.; Nguyen-Phanb, C.; Gardiner, A.; Crolld, T.; Roszakb, A.; Southall, J.; Jackson, P.; Vasileve, C.; Castro-Hartmanna, P.; Sadera, K.; Neil Hunter, C.; Cogdell, R. Cryo-EM structures of light-harvesting 2 complexes from *Rhodopseudomonas palustris* reveal the molecular origin of absorption tuning. *Proc. Natl. Acad. Sci. U. S. A*. **2022**, *119*, e2210109119.

(S3) Tani, K.; Nagashima, K. V. P.; Kanno, R.; Kawamura, S.; Kikuchi, R.; Hall, M.; Yu, L.-J.; Kimura, Y.; Madigan, M. T.; Mizoguchi, A.; *et al*. A previously unrecognized membrane protein in the *Rhodobacter sphaeroides* LH1-RC photocomplex. *Nat. Commun.* **2021**, *12*, 6300.

(S4) Yang, F.; Yu, L.-J.; Wang, P.; Ai, X.-C.; Wang, Z.-Y.; Zhang, J.-P. Effects of Aggregation on the Excitation Dynamics of LH2 from *Thermochromatium tepidum* in Aqueous Phase and in Chromatophores. *J. Phys. Chem. B* **2011**, *115*, 7906−7913.

(S5) Yu, L.-J.; Suga, M.; Wang-Otomo, Z.-Y.; Shen, J.-R. Structure of photosynthetic LH1-RC supercomplex at 1.9 Å resolution. *Nature* **2018**, *556*, 209−213.

(S6) Qian, P.; Croll, T. I.; Swainsbury, D. J. K.; Castro-Hartmann, P.; Moriarty, N. W.; Sader, K.; Hunter, C. N. Cryo-EM structure of the *Rhodospirillum rubrum* RC–LH1 complex at 2.5 Å. *Biochem*. *J*. **2021**, *478*, 3253−3263.

(S7) Yan Y.-H.; Wang G.-L.; Yue X.-Y.; Ma F.; Madigan, M.T.; Wang-Otomo, Z.-Y.; Zou, M.-J.; Yu, L.-J. Molecular structure and characterization of the *Thermochromatium tepidum* light-harvesting 1 photocomplex produced in a foreign host. *Biochim. Biophys. Acta.* **2024**,*1865*, 149050.

(S8) Hao, J.-F.; Yamano, N.; Qi, C.-H.; Zhang, Y.; Ma, F.; Wang, P.; Yu, L.-J.; Zhang, J.-P. Carotenoid-Mediated Long-Range Energy Transfer in the Light Harvesting–Reaction Center Complex from Photosynthetic Bacterium *Roseiflexus castenholzii*. *J. Phys. Chem. B* **2023**, *127*, 10360−10369.

(S9) Wang, X.-P.; Wang, G.-L.; Fu, Y.; Minamino, A.; Zou, M.-J.; Ma, F.; Xu, B.; Wang-Otomo, Z.-Y.; Kimura, Y.; Madigan, M. T.; et al. Insights into the divergence of the photosynthetic LH1 complex obtained from structural analysis of the unusual photocomplexes of *Roseospirillum parvum*. *Commun. Biol.* **2024**, *7*, 1658.

(S10) Zhang, Y.; Qi, C.-H.; Yamano, N.; Wang, P.; Yu, L.-J.; Wang-Otomo, Z.-Y.; Zhang, J.-P. Carotenoid Single-Molecular Singlet Fission and the Photoprotection of a Bacteriochlorophyll b-Type Core Light-Harvesting Antenna. *J. Phys. Chem. Lett.* **2022**, *13*, 3534−3541.

(S11) Yu, J.; Fu, L. M.; Yu, L. J.; Shi, Y.; Wang, P.; Wang-Otomo, Z. Y.; Zhang, J.-P. Carotenoid Singlet Fission Reactions in Bacterial Light Harvesting Complexes as Revealed by Triplet Excitation Profiles. *J. Am. Chem. Soc*. **2017**, *139*, 15984−15993.

(S12) Gao, R.-Y.; Zou, J.-W.; Shi, Y.-P.; Li, D.-H.; Zheng, J.; Zhang, J.-P. The Q-Band Energetics and Relaxation of Chlorophylls a and b as Revealed by Visible-to-Near Infrared Time-Resolved Absorption Spectroscopy. *J. Phys. Chem. Lett.* **2025**, *16*, 789−794.

(S13) Snellenburg, J. J.; Laptenok, S. P.; Seger, R.; Mullen, K. M.; Stokkum, I. H. M. Glotaran: A Java-Based Graphical User Interface for the R Packagetimp. *J. Stat. Softw*. **2012**, *49*,1−22.

(S14) Qi, C.-H.; Wang, G.-L.; Wang, F.-F.; Xin, Y.; Zou, M.-J.; Madigan, M. T.; Wang-Otomo, Z.-Y.; Ma, F.; Yu, L.-J. New Insights on the Photocomplex of *Roseiflexus castenholzii* Revealed from Comparisons of Native and Carotenoid-Depleted Complexes. *J. Biol. Chem.* **2023**, *299*, 105057.

(S15) Xin, J.; Shi, Y.; Zhang, X.; Yuan, X.; Xin, Y.; He, H.; Shen, J.; Blankenship, R. E.; Xu, X. Carotenoid Assembly Regulates Quinone Diffusion and the *Roseiflexus castenholzii* Reaction Center-Light Harvesting Complex Architecture. *eLife* **2023**, *12*, e88951.

(S16) Hao, J.-F.; Qi, C.-H.; Yu, B.-Y.; Wang, H.-Y.; Gao, R.-Y.; Yamano, N.; Ma, F.; Wang, P.; Xin, Y.-Y.; Zhang, C.-F.; et al. Light-Quality-Adapted Carotenoid Photoprotection in the Photosystem of *Roseiflexus castenholzii*. *J. Phys. Chem. Lett.* **2024**, *15*, 3470−3477.

(S17) Suzuki, H.; Hirano, Y.; Kimura, Y.; Takaichi, S.; Kobayashi, M.; Miki, K.; Wang, Z. Y. Purification, characterization and crystallization of the core complex from thermophilic purple sulfur bacterium *Thermochromatium tepidum*. *Biochim. Biophys. Acta.* **2007**, *1767*, 1057–1063.

(S18) Kakitani, Y.; Akahane, J.; Ishii, H.; Sogabe, H.; Nagae, H.; Koyama, Y. Conjugation-Length Dependence of the T_1 Lifetimes of Carotenoids Free in Solution and Incorporated into the LH2, LH1, RC, and RC-LH1 Complexes: Possible Mechanisms of Triplet-Energy Dissipation. *Biochemistry* **2007**, *46*, 2181−2197.

(S19) Permentier, H. P.; Neerken, S.; Schmidt, K. A.; Overmann, J.; Amesz, J. Energy transfer and charge separation in the purple non-sulfur bacterium *Roseospirillum parvum*. *Biochim. Biophys. Acta* **2000**, *1460*, 338–345.

(S20) Rondonuwu F. S.; Yokoyama K.; Fujii R.; Koyama Y. Cogdell R. J.; Watanabe Y. The role of the $1^1B_u^-$ state in carotenoid-to-bacteriochlorophyll singlet-energy transfer in the LH2 antenna complexes from *Rhodobacter sphaeroides G1C*, *Rhodobacter sphaeroides* 2.4.1, *Rhodospirillum molischianum* and *Rhodopseudomonas acidophila*, *Chemical Physics Letters* **2004**, *390*, 314–322.

(S21) Koyama Y.; Kakitani Y.; Watanabe Y. Photophysical properties and light-harvesting and photoprotective functions of carotenloids in bacterial photosynthesis: Structural selections, in: G. Renger (Ed.), Primary processes of photosynthesis - part 1: Principles and apparatus, RSC Publishing, Cambridge, 2008, pp. 151–201.

(S22) Angerhofer A.; Bornhauser F.; Gall A.; Cogdell R.J. Optical and optically detected magnetic-resonance investigation on purple photosynthetic bacterial antenna complexes. *Chem. Phys.* **1995**, *194*, 259–274.

(S23) Cong H.; Niedzwiedzki D. M.; Gibson G. N.; LaFountain A. M.; Kelsh R. M.; Gardiner A. T.; Cogdell R. J.; Frank H. A. Ultrafast timeresolved carotenoid to-bacteriochlorophyll energy transfer in LH2 complexes from photosynthetic bacteria, *J. Phys. Chem. B* **2008**, *112*, 10689–10703.

(S24) Zhang J.-P.; Fujii R.; Qian P.; Inaba T.; Mizoguchi T.; Koyama Y.; Onaka K.; Watanabe Y. Mechanism of the Carotenoid-to-Bacteriochlorophyll Energy Transfer via the S_1 State in the LH2 Complexes from Purple Bacteria, *J. Phys. Chem. B* **2000**, *104*, 3683–3691.

(S25) Noguchi T.; Hayashi H.; Tasumi M.; Factors controlling the efficiency of energy transfer from carotenoids to bacteriochlorophyll in purple photosynthetic bacteria, *Biochim. Biophys. Acta* **1990**, *1017*, 280–290.

(S26) Chi, S. C.; Mothersole, D. J.; Dilbeck, P.; Niedzwiedzki, D. M.; Zhang, H.; Qian, P.; Vasilev, C.; Grayson, K. J.; Jackson, P. J.; Martin, E. C.; Li, Y.; Holten, D.; Hunter, C. N. Assembly of Functional Photosystem Complexes in *Rhodobacter sphaeroides* incorporating Carotenoids from the Spirilloxanthin pathway, *Biochim. Biophys. Acta, Bioenerg.* **2015**, *1847*, 189−201.

(S27) Niedzwiedzki D. M.; Kobayashi M.; Blankenship R. E. Triplet excited state spectra and dynamics of carotenoids from the thermophilic purple photosynthetic bacterium *Thermochromatium tepidum*, *Photosynth Res*. **2011**, *107*, 177–186.

(S28) Niedzwiedzki D. M.; Fuciman M.; Kobayashi M.; Frank H. A,; Blankenship R. E. Ultrafast time-resolved spectroscopy of the light-harvesting complex 2 (LH2) from the photosynthetic bacterium *Thermochromatium tepidum*, *Photosynth Res*. **2011**, *110*, 49–60.

(S29) Nagashima K. V. P. *et al*. Probing structure–function relationships in early events in photosynthesis using a chimeric photocomplex, *PNAS* **2017**, *114*, 10906–10911.

(S30) Ma, F.; Kimura, Y.; Zhao, X.-H.; Wu, Y.-S.; Wang, P.; Fu, L.- M.; Wang, Z.-Y.; Zhang, J.-P. Excitation Dynamics of Two Spectral Forms of the Core Complexes from Photosynthetic Bacterium *Thermochromatium tepidum*, *Biophys. J*. **2008**, *95*, 3349−3357.